Optimal Multi-Objective Charging for Lithium-Ion Battery Packs: A Hierarchical Control Approach

Quan Ouyang[1], Jian Chen[1], *Senior Member, IEEE*, Jian Zheng[1], and Huazhen Fang[2], *Member, IEEE*

***Abstract*—Successful operation of a battery pack necessitates an effective charging management. This study presents a systematic investigation that blends control design with control implementation for battery charging. First, it develops a multi-module charger for a serially connected battery pack, which allows each cell to be charged independently by a modified isolated buck converter. Then, it presents the development of a two-layer hierarchical charging control approach to be run on this charger. The top-layer control schedules the optimal charging currents through a multi-objective optimization that takes into account user demand, cell equalization, temperature and operating constraints. The bottom-layer control is developed using the passivity theory to ensure that the charger can well track the scheduled charging current, and its stability is proven using the Lyapunov stability theory. Extensive simulation and experiments are provided to thoroughly validate the proposed charger and the hierarchical charging control approach.**

***Index Terms*—Optimal multi-objective charging, lithium-ion battery, hierarchical control, multi-module charger.**

I. INTRODUCTION

Rechargeable lithium-ion batteries are widely used in numerous applications stretching from green transportation to grid-scale energy storages, due to their advantages of high power density, low self-discharge and long cycle life [1], [2]. Since a single cell's voltage is inherently limited by its electrochemical characteristics, battery packs are built by connecting multiple cells in series to provide necessary high voltage. For the green transportation applications, the battery packs even consist of up to hundreds of serially connected cells to offer a voltage as high as several hundred volts. In these systems, battery management systems (BMSs) must be used to optimize the performance and extend the life time of battery packs [3], [4]. The past decades have witnessed plenty of investigations about the battery management schemes, such as state-of-charge (SOC) estimation [5]–[7], state-of-health (SOH) diagnosis [8], cell equalization [9], [10], and thermal management [11]. Another important yet less studied function of a BMS is the battery charging control. Improper charging, such as overcharging and charging with an excessive current, can lead to fast capacity fade, and even safety hazards. Meanwhile, too low charging speed will cause inconvenience in the battery use and eventually impair the consumers' confidence.

This work is supported by the National Natural Science Foundation of China (61433013) and the State Key Laboratory of Industrial Control Technology.

[1]Quan Ouyang, Jian Chen and Jian Zheng are with the State Key Laboratory of Industrial Control Technology, College of Control Science and Engineering, Zhejiang University, Hangzhou 310027, China (Corresponding author: Jian Chen, Email: jchen@zju.edu.cn).

[2]Huazhen Fang is with the Department of Mechanical Engineering, University of Kansas, Lawrence, KS 66045, the USA.

A review about the battery charging strategies is summarized in [12], which indicates that charging time, cell balance and temperature suppression are important factors to be considered in charging control for battery packs. The most commonly utilized battery charging method is the constant current-constant voltage (CC-CV) [13], in which a constant charging current is utilized until the battery's voltage reaches the specified value and then the mode is switched to a constant voltage charging. However, practical use of this method involves much empirical knowledge, e.g., deciding the magnitude of the current. Toward overcoming this issue, an optimal algorithm is proposed in [14] to determine the optimal constant current in the CC-CV method with consideration of charging time, energy loss, and temperature rise. Based on a coupled battery thermoelectric model, an advance optimal charging strategy is designed in [15] to develop the optimal CC-CV charging profile, which gives the best trade-off among the objectives of charging time, energy loss, and temperature rise. To improve the charging speed, a two-stage constant current charging scheme is formulated in [16], and an optimal five-step constant current charging strategy is proposed in [17]. In [18], an optimal voltage-based multistage constant current charging strategy is formulated and a multi-objective particle swarm optimization algorithm is employed to satisfy the different charging demands of charging time, charged capacity and energy loss with the impact of different weight combinations for balancing these demands analyzed. In [19], a dynamic data mining technique is designed for battery charging rule extraction to minimize charging time and overheating. A model predictive control based fast charging method is proposed in [20] with the aim of reducing the charging duration and the temperature increase. A dual-objective optimal charging method is designed in [21] that takes into account both charging time and energy efficiency. An optimal charging strategy is formulated in [22] to minimize the charging time while considering the temperature rise and other charging constraints. A model predictive control approach is proposed in [23] to manage battery charging operations in balancing charging time and temperature increase. In [24], a polarization based charging time and temperature rise optimization strategy for lithium-ion batteries is designed, and the genetic algorithm is adopted to search for the optimal charging current trajectories. A constrained generalized predictive control strategy is developed in [25] for the battery charging control with the aim of maintaining the temperature within a desirable range while delivering fast charging. A health-aware charging strategy is proposed in [26] to complete a fast charging task in the minimum amount of time while satisfying battery health-related constraints. Multi-objective biogeography-based optimization approaches are employed in [27] to search the

This article has been accepted for publication in a future issue of this journal, but has not been fully edited. Content may change prior to final publication. Citation information: DOI 10.1109/TII.2018.2825245, IEEE Transactions on Industrial Informatics

optimal charging patterns to balance the objectives of charging speed, energy conversion efficiency and temperature variations, and the pareto front analysis is provided for weight tuning among these objective functions. Despite the progress represented by the above strategies, a major deficiency in them is that the user demand is not involved in the charging control design. A battery charger can be more intelligent and conscious of battery health and bring a positive impact on user satisfaction if the user demand is taken under consideration in charging protocol design. It will be ideal if the charger can automatically adjust the charging process with an awareness of both health protection and user needs.

In this paper, a modified isolated buck converter based multi-module charger is designed for a serially connected battery pack. Based on this charger, a hierarchical control approach is proposed to enable optimal multi-objective charging of a battery pack. This approach features a two-layer design. The top-layer control consists of three aspects. First, it receives the user demand, which is expressed as the target SOC and charging time. Then, it formulates a multi-objective optimization problem that comprehensively takes into account the user demand, cell equalization, temperature suppression, and operating constraints in the charging process. Finally, it determines the optimal charging current profile by solving the optimization problem. In the bottom layer, an interconnection and damping assignment-passivity-based controller (IDA-PBC) is proposed to regulate the actual charging currents via the converters in the multi-module charger to track the scheduled current profile designed by the top layer.

The main contributions of this work lie in the following four aspects. 1) This study, as the first in the literature, systematically addresses charging control design. Most of the existing works only focus on charging current profile determination. By contrast, we begin with modeling the multi-module charger considered in this study using power electronics and circuit theory. Then, a user-involved hierarchical control approach is developed, which is composed of optimal charging current scheduling at the top layer and charging current tracking at the bottom layer. As a combination of physical process, control, and information communication, the presented systematic design makes the study closer to practice. 2) An optimal multi-objective charging problem is formulated to account for the user demand, cell equalization, and temperature effects simultaneously, and an optimal charging current scheduling algorithm is derived using a variable scheduling sampling period strategy to achieve computational efficiency. To the best of our knowledge, the cell equalizing issue has not been considered in the existing charging works about optimal charging, which restricts the capacity and performance of the battery pack. 3) An IDA-PBC is proposed to control the charging currents via the charger to track the current profile generated by the top-layer scheduling algorithm. We conduct a rigorous stability analysis for the closed-loop bottom-layer charging current tracking system using the Lyapunov theory, showing that its stability can be guaranteed. 4) Most of the optimal charging strategies are only based on simulation with experimental evaluation still absent. However, extensive experiments have been performed here to demonstrate the effectiveness of both the designed multi-module charger and the optimal multi-objective charging method.

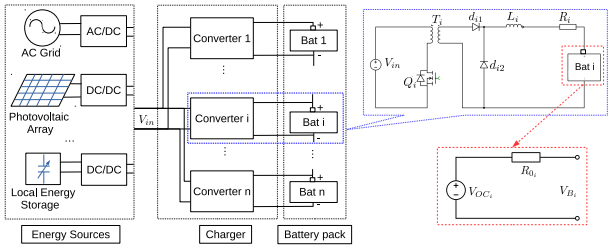

Fig. 1. Diagram of the multi-module charger for a serially connected lithium-ion battery pack.

The rest of this manuscript is organized in the following fashion. Section II represents the model of the battery charging system. In Section III, a two-layer hierarchical charging control approach is proposed. Related simulation and experimental results are included in Section IV to demonstrate the performance of the designed method, and conclusions are given in Section V.

II. CHARGING SYSTEM MODEL

Throughout this paper, we consider a general charging setting, where a variety of power sources, e.g., the AC grid, photovoltaic array, and local energy storage, can be used to charge a battery pack. As illustrated in Fig. 1, a multi-module charger is developed for an n-modular serially connected battery pack, which is composed of n modified isolated buck converters with each of them utilized to charge one cell. The modified isolated buck converter based charger has the advantage of easy implementation, reasonable size and cost, and allowing for integrated infrastructure and modular design. Moreover, the sweeping growth of the integrated circuit technology can significantly bring down the cost of battery chargers and potentially allow wide use of the proposed multi-module charger.

A. Battery Pack Modeling

The literature includes a number of battery models, which are reviewed in [28]. Among them, this work considers an internal resistance equivalent circuit model [29], which strikes a balance between accuracy and computational complexity. It is used to describe the dynamic behavior of each cell in the n-modular battery pack. It is noteworthy that this model is generally suitable for characterizing a battery operating within the normal temperature range. Hence, the effects of temperature on battery parameters are ignored here to simplify the analysis, design and implement of optimal charging control, though the proposed design can be extended to the case when a thermal model is included into this model. As shown in Fig. 1, the battery model is composed of a voltage source and a serially connected internal resistor. The i-th cell's terminal voltage can be expressed as:

$$V_{B_i} = V_{OC_i} + R_{0_i} I_{B_i} \tag{1}$$

This article has been accepted for publication in a future issue of this journal, but has not been fully edited. Content may change prior to final publication. Citation information: DOI 10.1109/TII.2018.2825245, IEEE Transactions on Industrial Informatics

where V_{B_i} and V_{OC_i} denote the i-th cell's terminal voltage and open circuit voltage (OCV), respectively; R_{0_i} is the internal resistor; I_{B_i} is the current of the i-th cell, which is defined positive when the cell is in the charging mode here. The i-th cell's OCV and internal resistance are nonlinear functions of its SOC as $V_{OC_i} = f_i(SOC_i)$ and $R_{0_i} = h_i(SOC_i)$, where SOC_i denotes the i-th cell's SOC, and the dynamics of which is given by

$$\frac{\mathrm{d}SOC_i}{\mathrm{d}t} = \frac{\eta_i}{Q_i} I_{B_i} \tag{2}$$

where η_i is the Coulombic efficiency, and Q_i is the i-th cell's capacity in Ampere-hour. The i-th cell's SOC is assumed to be known throughout this paper since it can be estimated by a large number of estimation algorithms with high accuracy, such as extended Kalman filter [5], neural network based nonlinear observer [7]. Based on (1)–(2), the model of the n-modular battery pack can be expressed as follows:

$$\begin{aligned} \dot{x} &= B_1 v \\ y &= f(x) + h(x) v \end{aligned} \tag{3}$$

where the state vector is $x = [x_1, \cdots, x_n]^T \triangleq [SOC_1, \cdots, SOC_n]^T \in \mathbb{R}^n$; the input and output are $v = [v_1, \cdots, v_n]^T \triangleq [I_{B_1}, \cdots, I_{B_n}]^T \in \mathbb{R}^n$ and $y = [y_1, \cdots, y_n]^T \triangleq [V_{B_1}, \cdots, V_{B_n}]^T \in \mathbb{R}^n$; $f(\cdot) = [f_1(\cdot), \cdots, f_n(\cdot)]^T \in \mathbb{R}^n$; $B_1 = diag\{\frac{\eta_1}{Q_1}, \cdots, \frac{\eta_n}{Q_n}\} \in \mathbb{R}^{n\times n}$ and $h(\cdot) = diag\{h_1(\cdot), \cdots, h_n(\cdot)\} \in \mathbb{R}^{n\times n}$ with $diag\{\cdot\}$ denoting the diagonal matrix.

B. Multi-Module Charger Modeling

We propose the design of a modified isolated buck converter, which consists of a transformer T_i, an inductor L_i, a MOSFET Q_i, and two diodes d_{i1} and d_{i2}, as illustrated in Fig. 1. Compared with a traditional buck converter, this one does not need the capacitor in the output port. When maintained in the continuous conduction mode [30], the model of the i-th modified isolated buck converter is formulated as:

$$\frac{\mathrm{d}I_{B_i}}{\mathrm{d}t} = \frac{D_i}{L_i} V_{in} - \frac{V_{B_i}}{L_i} - \frac{I_{B_i} R_i}{L_i} \tag{4}$$

where V_{in} denotes the rectified DC input voltage, R_i is a current sense resistor, V_{B_i} and I_{B_i} represent the i-th cell's terminal voltage and charging current, and D_i ($0 \le D_i \le 1$) is the duty cycle of the pulse width modulation (PWM) signal applied to MOSFET Q_i. Based on (4), the model of the multi-module charger can be represented as follows:

$$\dot{v} = -Av + C_1 u - C_2 y \tag{5}$$

with $A = diag\{\frac{R_1}{L_1}, \cdots, \frac{R_n}{L_n}\} \in \mathbb{R}^{n\times n}$, $C_1 = diag\{\frac{V_{in}}{L_1}, \cdots, \frac{V_{in}}{L_n}\} \in \mathbb{R}^{n\times n}$, $C_2 = diag\{\frac{1}{L_1}, \cdots, \frac{1}{L_n}\} \in \mathbb{R}^{n\times n}$, where $u = [u_1, \cdots, u_n]^T \triangleq [D_1, \cdots, D_n]^T \in \mathbb{R}^n$ is the control variable.

Remark 1: For traditional chargers that provide the same charging current to all cells in the battery pack, the charging process has to be terminated when one of the cells reach the upper SOC threshold to avoid overcharging, even though other cells are not fully charged. This will lead to significantly conservative use of the battery pack. In our proposed multi-module charger, each cell is independently charged by a modified isolated buck converter. This design will bring two benefits that distinguish itself from the current literature. First, the charging control can be enforced to an individual cell level, giving us more control authority over the charging process. Second, with the capability of controlling individual cells, we can delicately regulate the charging process for each cell to balance the SOC toward the same level.

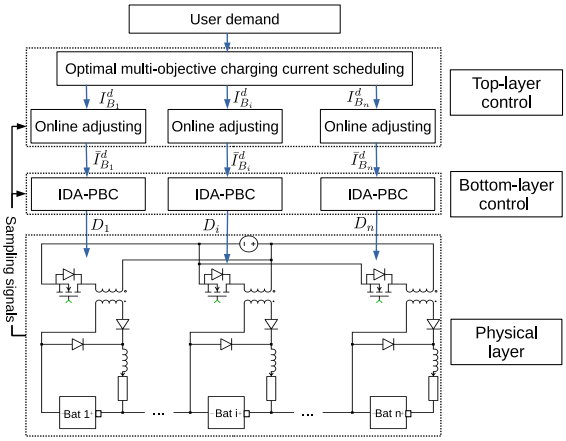

Fig. 2. Block diagram of the overall battery charging process.

C. Charging System Modeling

The overall charging system model consists of the model of the battery pack (3) and the model of the multi-module charger (5), where the charger system's output is the input of the battery pack system. The duty cycle vector u in (5) is controlled to regulate the charging current vector v to make the cells' SOC vector x in (3) reach its desired value. Since the modified isolated buck converter based charger has much faster transient response than the dynamics of the battery pack, the control strategy can be divided into two layers, the top layer for generating the optimal charging current profile and the bottom layer for controlling the charger to provide the desired charging currents. Next, we will present the development of such a hierarchical control strategy.

III. HIERARCHICAL CONTROL STRATEGY FOR THE CHARGING SYSTEM

In this section, we first formulate the objectives and constraints of the charging process. Then, we propose a hierarchical control strategy to ensure that the charging system can satisfy these objective and constraints. As illustrated in Fig. 2, the overall hierarchical control strategy comprises two layers. The top-layer control is to schedule the optimal charging currents by considering user demand, cell equalization, temperature buildup, and constraints in the charging process. The bottom-layer control is to regulate the charging currents provided by the designed multi-module charger to track the desired charging currents designed by the top layer.

To better schedule the optimal charging currents, the battery pack model (3) is discretized by holding the charging currents constant during each scheduling sampling interval. The discrete-time model is given by

$$\begin{aligned} x(k+1) &= x(k) + Bv(k) \\ y(k) &= f(x(k)) + h(x(k))v(k) \end{aligned} \tag{6}$$

where $B = diag\{\frac{\eta_1 T}{Q_1}, \cdots, \frac{\eta_n T}{Q_n}\} \in \mathbb{R}^{n\times n}$ with the scheduling sampling period T.

A. Charging Objectives

Charging task: For a battery pack with the initial cells' SOC vector $x(0) = x_0$, the user can define the target SOC and the charging duration according to the next need:

$$x_s(N) = \Gamma_{set} 1_n \quad \text{with} \quad T_{set} = NT \tag{7}$$

where Γ_{set} and T_{set} are the desired SOC and the demanded charging duration of the battery pack, respectively; 1_n denotes a column vector with n ones and N is the sampling step number. Toward meeting this charging objective, it is intended to minimize the difference between $x(N)$ and $x_s(N)$, and the corresponding cost function can be expressed as:

$$J_x = \tfrac{1}{2}(x(N) - x_s(N))^T (x(N) - x_s(N)). \tag{8}$$

A hard constraint of the terminal state vector $x(N) = x_s(N)$ is adopted in [31] to make the cells' SOCs at the end of the charging process equal to their target value. But the user settings may not be achievable in practice, e.g., the battery pack cannot be fully charged with a very short charging duration of the user demand even if we persistently charge the battery with the maximum allowed charging current. In these cases, it is not suitable to use the hard constraint in our charging current scheduling algorithm, since it may result in an infeasible problem with the solution set being empty under all the charging constraints. By using the cost function (8) rather than the hard constraint $x(N) = x_s(N)$, such nonsense cases can be effectively avoided such that a feasible solution always exists to minimize J_x and drive $x(N)$ toward to the desired $x_s(N)$ to the greatest extent with satisfying all charging constraints.

Cell equalization: In a battery pack, the energy imbalance among cells exists due to the imperfect battery manufacturing technology and spatially uneven temperature distribution. The cells' lowest/highest SOC restricts the usable/rechargeable capacity of the entire battery pack. Hence, the effective capacity of the battery pack can be crucially enhanced by equalizing the SOC of each cell to a same level. The cell equalization issue can be recast as minimizing the cells' SOC difference $||x(k) - \bar{x}(k)||$ in the charging process, where $||\cdot||$ denotes the 2-norm and $\bar{x}(k) = \frac{1}{n} 1_n 1_n^T x(k)$ stands for the average SOC vector of the battery pack. Hence, the cost function for cell equalization can be formulated as:

$$J_e = \tfrac{1}{2N} \sum_{k=1}^{N} x^T(k) D^T D x(k) \tag{9}$$

with $D = I_n - \frac{1}{n} 1_n 1_n^T$, where I_n denotes the identity matrix with dimensions of $n \times n$. In (9), $\frac{1}{N}$ is included to make the order of magnitude of J_e comparable to J_x in (8).

Temperature effects: Based on [14], the temperature dynamics of the i-th $(1 \le i \le n)$ cell can be modeled as:

$$\begin{aligned} T_{e_i}(k+1) = T_{e_i}(k) - b_{i1}(T_{e_i}(k) - T_a) + b_{i2} v_i^2(k) \\ + \sum_{j=1}^{n} r_{ij}(T_{e_j}(k) - T_{e_i}(k)) \end{aligned} \tag{10}$$

where $T_{e_i}(k)$ is the i-th cell's lumped temperature, T_a denotes the ambient temperature, r_{ij} represents the coefficient of the heat transfer from the j-th cell to the i-th cell in the battery pack, b_{i1} and b_{i2} are coefficients relevant to heat transfer and Joule heating, respectively. The temperature rise over a sampling period can be defined as $\Delta T_e(k) = T_e(k+1) - T_e(k)$, where $T_e(k) = [T_{e_1}(k), \cdots, T_{e_n}(k)]^T \in \mathbb{R}^n$. Based on (10), it can be obtained that

$$\Delta T_e(k) = A_e T_e(k) + B_{e1} T_a + B_{e2} \underline{v}(k) \tag{11}$$

where $A_e = [-b_{11} + r_{11} - \sum_{j=1}^{n} r_{1j}, r_{12}, \cdots r_{1n};\ r_{21}, -b_{21} + r_{22} - \sum_{j=1}^{n} r_{2j}, \cdots, r_{2n};\ \cdots;\ r_{n1}, r_{n2}, \cdots, -b_{n1} + r_{nn} - \sum_{j=1}^{n} r_{nj}] \in \mathbb{R}^{n\times n}$, $B_{e1} = [b_{11}, b_{21}, \cdots, b_{n1}]^T \in \mathbb{R}^n$, $B_{e2} = diag\{b_{12}, b_{22}, \cdots, b_{n2}\} \in \mathbb{R}^{n\times n}$, and $\underline{v}(k) = [v_1^2(k), \cdots, v_n^2(k)]^T \in \mathbb{R}^n$. The cells' temperature rises can be restrained by utilizing (11) to construct a cost function. However, because r_{ij}, b_{i1}, and b_{i2} in (11) are difficult to be accurately identified in practice, it is hard to get the precise temperature rise. In addition, using a model as in (11) will significantly increase the computational cost when addressing the charging optimization problem to be formulated later. However, based on (11), it is observed that the cells' temperature rises depend on the square of their charging currents. To ensure that the cells' temperature rises within the normal operating range, the charging currents should not be too large. Hence, to simplify the thermal rise management issue, we seek to constrain the magnitude of the square of charging current rather than the temperature rise directly. This leads us to a cost function as follows:

$$J_v = \tfrac{1}{2N} \sum_{k=0}^{N-1} v^T(k) v(k). \tag{12}$$

Usually, the battery pack's temperature will not exceed its limitation in normal situations when the cells' currents and terminal voltages are strictly less than the maximum allowed values. Hence, we do not need the hard temperature restriction in the charging current design algorithm but use (12) to ensure that the battery pack's temperature rise does not become too high. For an extreme situation when the cells' temperatures exceed their limitation, the charging process is terminated for thermal safety.

Multi-objective formulation: For the optimal charging current scheduling issue, the user demand, the cell equalization, and the thermal effect should all be taken into consideration. To balance them, the following quadratic multi-objective cost function is formulated by combining (8), (9), and (12) as:

$$J(x(k), v(k)) = \gamma_1 J_x + \gamma_2 J_e + \gamma_3 J_v \tag{13}$$

where $\gamma_1 \ge 0$, $\gamma_2 \ge 0$, and $\gamma_3 \ge 0$ are the trade-off weights.

B. Charging Constraints

To guarantee the stability the battery pack system and extend its life time, the following three constraints should be satisfied in the charging process: the cells' SOC limitations, the charging current restrictions, and the terminal voltage constraints.

SOC limitations: To avoid overcharging of the battery pack, the cells' SOCs should be in the bound below the upper limitation x_u that

$$\chi = \{x(k) \in \mathbb{R}^n | x(k) \leq x_u\}. \tag{14}$$

Charging current restrictions: Since excessive charging currents, which are defined as the charging currents larger than the maximum allowed values, are harmful for batteries, the cells' charging currents should be maintained within a suitable range ν that

$$\nu = \{v(k) \in \mathbb{R}^n | 0_n \leq v(k) \leq v_M\} \tag{15}$$

where $v_M \in \mathbb{R}^n$ denotes the cells' maximum allowed charging current vector, and 0_n denotes the vector with n zeros.

Terminal voltage constraints: The cells' terminal voltages should not exceed the upper voltage limitation. From (3), for the battery pack, it should satisfy

$$f(x(k)) + h(x(k))v(k) \leq y_M \tag{16}$$

where $y_M \triangleq V_{max} 1_n \in \mathbb{R}^n$ with V_{max} the cells' maximum allowed terminal voltage.

C. Top-Layer Control: Optimal Charging Current Scheduling

With considering the multi-objective (13) and the constraints (14)–(16) in the charging process, the charging current scheduling problem can be transformed to a constrained optimization issue as follows:

$$\begin{aligned} \underset{v(0),\cdots,v(N-1)}{\text{minimize}} \quad & J(x(k), v(k)) \\ \text{subject to} \quad & x(k+1) = x(k) + Bv(k), \quad x(0) = x_0 \\ & f(x(k)) + h(x(k))v(k) \leq y_M \\ & x(k) \leq x_u, \quad v(k) \in \nu. \end{aligned} \tag{17}$$

According to (17), it yields $x(k) = x_0 + \sum_{j=0}^{k-1} Bv(j)$, which can be rewritten as $x(k) = x_0 + BH_k U$ by defining $U \triangleq [v^T(0), \cdots v^T(N-1)]^T \in \mathbb{R}^{nN}$ and $H_k \triangleq [\Upsilon_k, \Theta_k] \in \mathbb{R}^{n \times nN}$ with $\Upsilon_k = [I_n, \cdots, I_n] \in \mathbb{R}^{n \times kn}$ and $\Theta_k = [0_{n\times n}, \cdots, 0_{n\times n}] \in \mathbb{R}^{n\times(N-k)n}$. Then, the constrained optimization issue (17) can be rewritten as the following form:

$$\begin{aligned} \underset{U}{\text{minimize}} \quad & J_1(U) + \tau \\ \text{subject to} \quad & F(U) + G(U)U \leq Y_M \\ & MU \leq X_C, \quad \Phi U \leq U_M \end{aligned} \tag{18}$$

with the auxiliary variables

$J_1(U) = x_0^T \Psi_1 U - x_s^T \Psi_2 U + U^T \Psi_3 U$

$\tau = \frac{\gamma_1}{2}(x_0^T x_0 - 2x_0^T x_s(N) + x_s^T(N) x_s(N)) + \frac{\gamma_2}{2} x_0^T D^T D x_0$

$\Psi_1 = \gamma_1 B H_N + \frac{\gamma_2}{N} \sum_{j=1}^{N} D^T D B H_j, \quad \Psi_2 = \gamma_1 B H_N$

$\Psi_3 = \frac{\gamma_1}{2} H_N^T B^T B H_N + \frac{\gamma_2}{2N} \sum_{j=1}^{N} H_j^T B^T D^T D B H_j + \frac{\gamma_3}{2N} I_{nN}$

where U is the optimization variable; $Y_M \in \mathbb{R}^{nN}$, $X_C \in \mathbb{R}^{nN}$, $F(U) \in \mathbb{R}^{nN}$, $G(U) \in \mathbb{R}^{nN \times nN}$, $M \in \mathbb{R}^{nN \times nN}$, $\Phi \in \mathbb{R}^{2nN \times nN}$, and $U_M \in \mathbb{R}^{2nN}$ are defined as:

$Y_M = [y_M^T, \cdots, y_M^T]^T$, $X_C = [(x_u - x_0)^T, \cdots, (x_u - x_0)^T]^T$

$F(U) = [f^T(x_0 + DH_1 U), \cdots, f^T(x_0 + DH_N U)]^T$

$G(U) = diag\{h(x_0 + DH_1 U), \cdots, h(x_0 + DH_N U)\}$

$M = [(BH_1)^T, \cdots (BH_N)^T]^T$, $\Phi = [I_{nN}, -I_{nN}]^T$

$U_M = [v_M^T, \cdots, v_M^T, 0_n^T, \cdots, 0_n^T]^T$.

Since τ is a constant, it can be eliminated for solving the optimization issue (18). By introducing a convex barrier function [32] to replace the inequality constraints, the constrained optimization (18) can be transformed as:

$$\underset{U}{\text{minimize}} \; J_1(U) - \frac{1}{\mu_1} \sum_{j=1}^{4nN} log(-g_j(U)) \tag{19}$$

where $-\sum_{j=1}^{4nN} log(-g_j(U))$ represents the logarithmic barrier function, μ_1 is a positive parameter, and $g_j(U)$ is the j-th element of the vector $g(U) \in \mathbb{R}^{4nN}$ given as:

$$g(U) = \begin{bmatrix} F(U) + G(U)U - Y_M \\ MU - X_C \\ \Phi U - U_M \end{bmatrix}. \tag{20}$$

An interior point based algorithm in [32] can be employed to solve the optimization problem (19), and the sequence of the optimal charging currents $I_{B_i}^d$ $(1 \leq i \leq n)$ can be obtained by off-line computation.

Variable scheduling sampling period: The scheduling sampling period is important for the success of the charging control approach when applied in practice. Large scheduling sampling period T implies a big model discretization error of (6). As a result, the cells' actual states may implicitly exceed the limitations when the cells are charged approaching the fully-charged states. However, if the scheduling sampling period is small, it will require more computational cost, which is not desirable for practical implementation. For a trade-off between the performance and the amount of calculation, a variable scheduling sampling period is adopted as:

$$T = \begin{cases} T_1 & x(k) \leq x_T \\ T_2 & x(k) > x_T \end{cases} \tag{21}$$

where $x_T = \Gamma_T 1_n$ with Γ_T is a preset SOC that is close to the fully-charged state, T_1 and T_2 are scheduling sampling periods that can be designed by considering both the practical accuracy need of the discrete-time battery model and the computational complexity of the charging current scheduling algorithm. As shown in (21), a large T_1 is chosen to reduce the computational amount when the cells' SOCs are less than x_T and the scheduling sampling period is changed to a small value T_2 to avoid large model discretization error when the cells' SOCs increase to be larger than x_T. The detailed method for the implementation of the variable scheduling sampling period is described in Algorithm 1.

Algorithm 1:

- 1) Set the user demand Γ_{set}, T_{set}, the intial cells' SOC vector x_0, the preset SOC vector x_T, and the scheduling sampling period $T = T_1$. The step number is $N_1 = \frac{T_{set}}{T_1}$.
- 2) Run the interior point algorithm and get the scheduled cells' charging current vector $v(k)$ $(k = 0, \cdots, N_1 - 1)$ and the updated SOC vector $x(k)$ $(k = 1, \cdots, N_1)$.
- 3) If $\Gamma_{set} 1_n \leq x_T$, stop and output $v(k)$ $(k = 0, \cdots, N_1 - 1)$. Otherwise, increase k from 1 to N_1 to find a k_1 that satisfies $k_1 = max\{k : x(k) \leq x_T\}$. Record $v(k)$

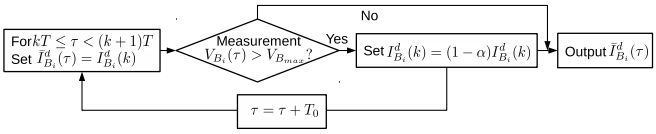

Fig. 3. Flow chart of the on-line charging current adjustment strategy.

$(k = 0, \cdots, k_1 - 1)$ and set $x(k_1)$ as the new initial cells' SOC vector.

- 4) Change the scheduling sampling period $T = T_2$, and the step number is $N_2 = \frac{T_{set} - k_1 T_1}{T_2}$. Run the interior point algorithm again and get the designed cells' charging current vector $v(k)$ $(k = k_1, \cdots k_1 + N_2 - 1)$.
- 5) Terminate and output $v(k)$ $(k = 0, \cdots, k_1 - 1, k_1 \cdots k_1 + N_2 - 1)$ by combining the results from Step 3) and Step 4).

On-line adjustment of desired charging currents: Due to the existence of the bias and disturbance between the model in the charging current scheduling algorithm and the actual characteristics of the battery pack in practice, the i-th $(1 \le i \le n)$ cell's terminal voltage V_{B_i} may exceed its upper bound with the scheduled optimal charging currents $I^d_{B_i}$. As shown in (16), the terminal voltage increases with the charging current, i.e., high charging current will cause large terminal voltage. Hence, once the i-th cell's measured terminal voltage V_{B_i} is larger than its maximum allowed value $V_{B_{max}}$, the charging current should be reduced to make V_{B_i} fall. Based on this idea, an on-line charging current adjusting strategy is proposed that reduces the actual desired charging current by a specific rate α $(0 < \alpha < 1)$ until the i-th cell's measured terminal voltage V_{B_i} is reduced to meet the constraints (16). The strategy is illustrated in Fig. 3, in which $\bar{I}^d_{B_i}$ is the i-th cell's desired charging current after adjustment and set as the tracking value of the bottom-layer controller, T_0 is the control sampling period. Note that a larger adjusting rate α means faster tuning speed, which can result in less overvoltage duration but may bring excessive reduction of $\bar{I}^d_{B_i}$ that comprises the charging process performance. Through experimental validation, a suitable α can be selected that brings a fast tuning speed to ensure the cells' terminal voltage constraints without compromising much performance. Since the overvoltage phenomenon only occurs in the case that the cells are approaching full charge, the actual cells' SOC trajectories are still near the scheduled ones.

D. Bottom-Layer Control: Charging Current Tracking

The objective of the bottom-layer controller is to make the actual charging currents through the multi-module charger track their desired values $\bar{I}^d_{B_i}$ $(1 \le i \le n)$ designed by the top layer. From an energy-based perspective [30], we can define the Hamiltonian function of the charger to denote the total energy stored in the system as:

$$H(v) = \frac{1}{2} v^T C v \tag{22}$$

with $C = diag\{L_1, \cdots, L_n\} \in \mathbb{R}^{n \times n}$. Based on (5) and (22), the model of the charger can be rewritten as:

$$\dot{v} = -A_1 \frac{\partial H(v)}{\partial v} + C_1 u - C_2 y \tag{23}$$

with $A_1 = diag\{\frac{R_1}{L_1^2}, \cdots, \frac{R_n}{L_n^2}\} \in \mathbb{R}^{n \times n}$, where y is considered as a measurable disturbance vector here. To ensure the charging currents v_i $(1 \le i \le n)$ tracking their desired values $\bar{I}^d_{B_i}$, an IDA-PBC is proposed for the system (23), which assigns a desired energy function that has a minimum at the desired equilibrium point by modifying the control input [30]. Here, we define the desired total energy function as:

$$H_d(v) = \tfrac{1}{2}(v - v^d)^T C (v - v^d) \tag{24}$$

where $v^d = [\bar{I}^d_{B_1}, \cdots, \bar{I}^d_{B_n}]^T \in \mathbb{R}^n$. Since the desired charging current is a slow changing signal compared with the converter's fast dynamics, the derivative of the desired charging current can be assumed to zero and thus $\dot{v}^d = 0_n$. From (24), it shows that $H_d(v) \ge 0$ and $H_d(v) = 0$ if and only if $v = v^d$ since C is positive definite. Assuming that a control input $u = \beta(v, v^d)$ can be found that makes the closed-loop system of (23) satisfy

$$\dot{v} = -R_d \frac{\partial H_d(v)}{\partial v} \tag{25}$$

where $R_d = diag\{R_{d_1}, \cdots, R_{d_n}\} \in \mathbb{R}^{n \times n}$ is a designed positive definite matrix. According to (23) and (25), it yields

$$-R_d \frac{\partial H_d(v)}{\partial v} = -A_1 \frac{\partial H(v)}{\partial v} + C_1 \beta(v, v^d) - C_2 y. \tag{26}$$

From (26), the control input can be deduced as:

$$\begin{aligned} u &= \beta(v, v^d) \\ &= C_1^{-1}((A_1 - R_d)Cv + R_d C v^d + C_2 y) \end{aligned} \tag{27}$$

where C_1^{-1} denotes the inverse matrix of C_1.

Stability proof: A Lyapunov candidate function is selected as:

$$V = H_d(v) \tag{28}$$

where $H_d(v)$ is seen in (24). According to (22)–(27), the derivative of (28) satisfies

$$\dot{V} = \frac{\partial H_d(v)}{\partial v} \dot{v} \le -P \tilde{v}^2 \tag{29}$$

where $P = C R_d C$, $\tilde{v} = (v - v^d)$. Since P is positive definite, $\dot{V} \le 0$ and $\dot{V} = 0$ if and only if $v = v^d$. According to the LaSalle's invariance principle [33], $v \to v^d$. Hence, the stability proof of the closed-loop bottom-layer charging current tracking system is achieved.

Since the modified buck converters are actually independently controlled, the controller (27) can be rewritten as n distributed IDA-PBCs:

$$u_i = \frac{(R_i - R_{d_i} L_i^2) v_i + R_{d_i} L_i^2 v_i^d + V_{B_i}}{V_{in}} \tag{30}$$

for $1 \le i \le n$, where R_{d_i} is chosen to make the duty cycle u_i within the set $[0, 1]$.

Remark 2: From the stability proof above, the actual charging currents via the charger are guaranteed to asymptotically track their desired values as scheduled by the top layer. Since the charging constraints of the battery pack system can be guaranteed with the scheduled charging currents by

This article has been accepted for publication in a future issue of this journal, but has not been fully edited. Content may change prior to final publication. Citation information: DOI 10.1109/TII.2018.2825245, IEEE Transactions on Industrial Informatics

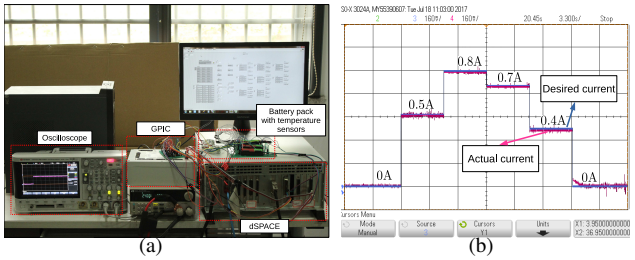

Fig. 4. (a) Experimental test bench, (b) desired and actual current responses of the modified buck converter with the IDA-PBC.

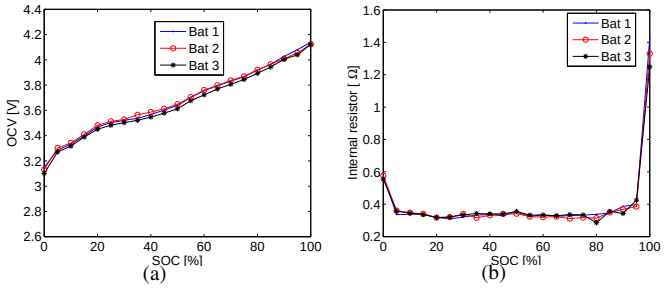

Fig. 5. (a) Relationship between the cells' OCVs and SOCs, (b) mapping from the SOCs to the internal resistors of the cells.

the top layer, the stable battery charging can be achieved with the actual charging currents controlled by the proposed hierarchical approach.

IV. SIMULATION AND EXPERIMENTAL RESULTS

In this section, the proposed battery charger and the optimal charging current scheduling approach are validated through extensive simulation and experiments. As illustrated in Fig. 4(a), the experimental bench mainly includes a battery pack composed of three serially connected PowerFocus 18650 lithium-ion batteries, a set of dSPACE, three OMEGA temperature sensors, and an NI general purpose inverter controller (GPIC) Single-Board 9683. With several charging tests, the capacities of the cells are identified as $Q_1 = 2.341$ Ah, $Q_2 = 2.387$ Ah, and $Q_3 = 2.379$ Ah, respectively. The relationships between the cells' OCVs and SOCs are illustrated in Fig. 5(a), and the cells' internal resistances are shown in Fig. 5(b). The cells' internal resistances are approximately constant within the SOC range $[5\%, 95\%]$, but increase sharply when the cells' SOCs are close to fully-charged states $[95\%, 100\%]$. It implies that the cells' terminal voltages may easily exceed their limitations with the SOCs larger than 95%. Hence, in the variable scheduling sampling method, the preset SOC is set as $\Gamma_T = 95\%$. The sampling periods are selected as $T_1 = 600$ s, $T_2 = 60$ s. The upper bound of the cells' SOCs is $x_u = 100\%$, and the cells' maximum allowed terminal voltage is set as $V_{max} = 4.2$ V. The on-line adjustment of desired charging currents is constructed on the GPIC. If the cell's measured terminal voltage is larger than 4.2 V, the desired charging current is reduced by 5% with the control sampling period $T_0 = 0.5$ s until the cell's measured terminal voltage is pushed below the constraints (16). Note that other suitable parameters can also be assigned, depending on the needs and performance in practice.

The modified isolated buck converter based multi-module charger is modeled in the dSPACE through real-time simulation with inductor $L_i = 0.01$ H $(1 \leq i \leq 3)$, non-ideal transformer T_i, MOSFET Q_i with internal diode resistance $0.1\ \Omega$ and FET resistance $0.01\ \Omega$, diodes d_{i1} and d_{i2} with snubber resistances $500\ \Omega$. The DC input voltage is $V_{in} = 24$ V, and the frequency of the PWM signal applied on the MOSFETs is set as 5 KHz. The current sense resistor is chosen as $R_i = 1\ \Omega$. A preliminary experiment is conducted first to verify the performance of the modified isolated buck converter. The desired and actual charging current responses of the modified buck converter with the IDA-PBC are shown in Fig. 4(b), where the actual current is obtained by measuring the current sense resistor's voltage through the Keysight oscilloscope. The experimental result demonstrates that the designed IDA-PBC can make the actual charging current through the converter track the desired value at a satisfactory level.

A. Simulation Results

MATLAB based simulations are conducted for a 10-modular serially connected battery to validate the usefulness of the proposed optimal charging current scheduling algorithm. The cells' capacities are randomly selected, varying from 1.90 Ah to 2.10 Ah with $[Q_1, \cdots, Q_{10}] = [2.07$ Ah,1.91 Ah,1.93 Ah, 1.96 Ah,1.97 Ah,2.09 Ah,2.06 Ah, 1.99 Ah,1.95 Ah,2.10 Ah$]$. The cells' initial SOCs are randomly given as $[x_1(0), \cdots, x_{10}(0)] = [12\%, 20\%, 18\%, 19\%, 16\%, 14\%, 17\%, 10\%, 15\%, 11\%]$. The initial cells' SOC difference is $||x(0) - \bar{x}(0)|| = 10.28\%$. The cells' maximum allowed charging current is chosen as 3 C-rate. Without loss of generality, the OCVs and the internal resistances of the first, fourth, seventh, and tenth/second, fifth, and eighth/third, sixth, and ninth cells in the simulation are chosen as the same as the model parameters of the actual battery cell 1/2/3 in the experiment (fitted by interpolation) shown in Fig. 5. The ambient temperature is set as $25\ ^{\circ}$C and the temperature influence coefficients b_{i1} and b_{i2} $(1 \leq i \leq 10)$ are chosen as the same in [14]. To demonstrate the performance of our designed charging strategy, the desired SOC of the battery pack is chosen as $\Gamma_{set} = 100\%$, and the charging durations are set as $T_{set} = 60$ min, $T_{set} = 120$ min, and $T_{set} = 180$ min, respectively. The weights of the cost function (13) in the optimal charging current scheduling algorithm are chosen as $\gamma_1 = 1000$, $\gamma_2 = 5$, and $\gamma_3 = 0.01$.

The simulation results are illustrated in Fig. 6 in terms of the cells' SOCs, charging currents, terminal voltages, and temperatures. As shown in Figs. 6(b), 6(f), and 6(j), the designed optimal charging currents can be adjusted with different user settings in our proposed charging strategy. For a short and tight charging duration of 60 min, large charging currents are designed to charge the cells' SOCs close to the desired SOC with high cells' temperatures (maximum temperature of 29.01°C in the charging process). However, small charging currents are used for a long and sufficient charging duration of 180 min, which satisfies the charging demand while resulting in relatively low temperatures (maximum temperature of 26.81°C). The cells' terminal voltage responses are shown in

This article has been accepted for publication in a future issue of this journal, but has not been fully edited. Content may change prior to final publication. Citation information: DOI 10.1109/TII.2018.2825245, IEEE Transactions on Industrial Informatics

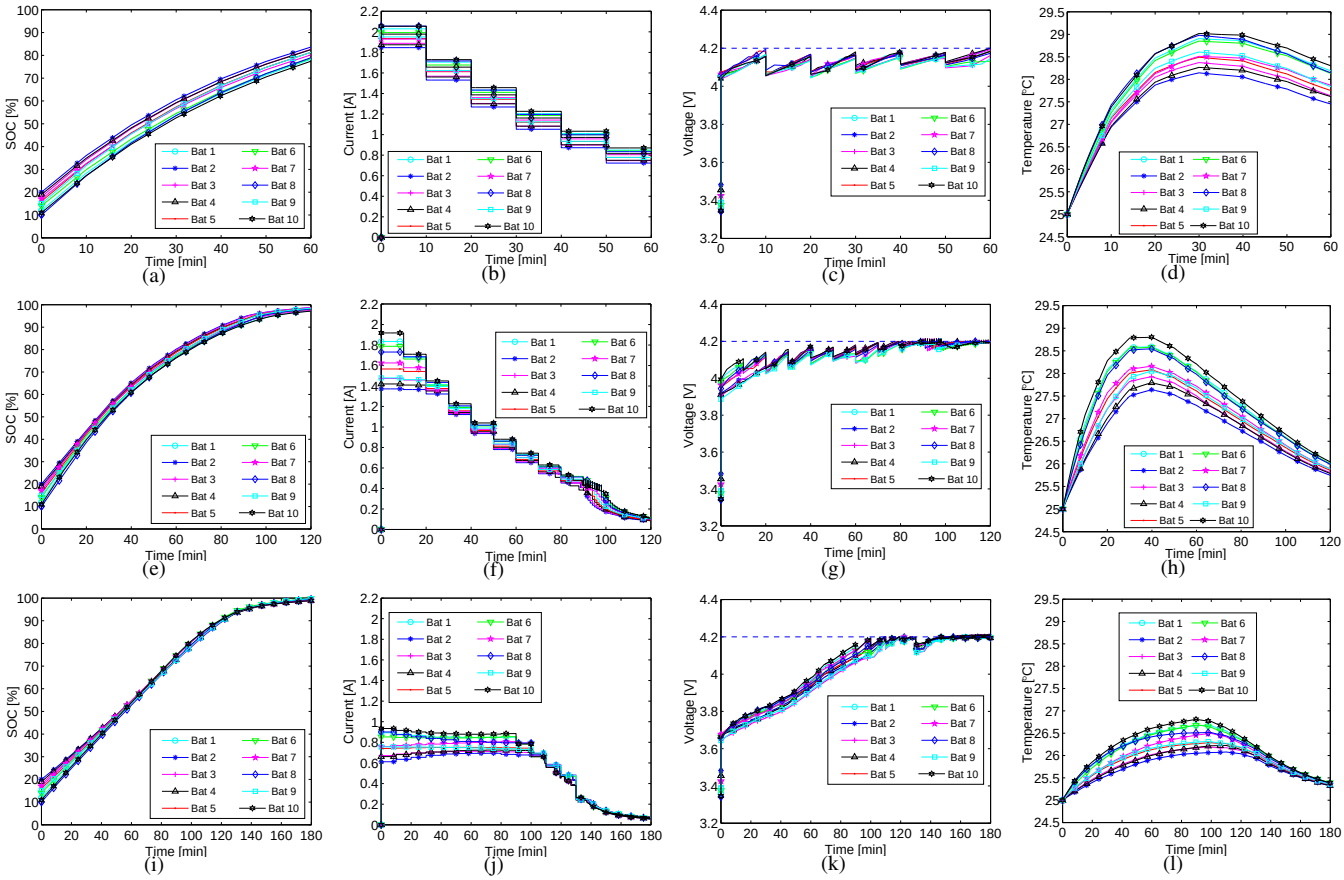

Fig. 6. Simulation results of cells' (a) SOCs with $T_{set} = 60$ min, (b) charging currents with $T_{set} = 60$ min, (c) terminal voltages with $T_{set} = 60$ min, (d) temperatures with $T_{set} = 60$ min, (e) SOCs with $T_{set} = 120$ min, (f) charging currents with $T_{set} = 120$ min, (g) terminal voltages with $T_{set} = 120$ min, (h) temperatures with $T_{set} = 120$ min, (i) SOCs with $T_{set} = 180$ min, (j) charging currents with $T_{set} = 180$ min, (k) terminal voltages with $T_{set} = 180$ min, (l) temperatures with $T_{set} = 180$ min.

TABLE I
SIMULATION RESULTS FOR DIFFERENT USER SETTINGS

	Average SOC	SOC difference	Maximum temperature
Initial	15.2%	10.83%	–
60 min charging	80.5%	6.67%	29.01°C
120 min charging	98.01%	1.85%	28.8°C
180 min charging	99.36%	1.28%	26.81°C

Figs. 6(c), 6(g), and 6(k), which can satisfy the constraints (16) well with the designed charging currents. The cells' average SOC and SOC difference at the end of the charging process, and the maximum temperature during the charging process are calculated as shown in TABLE I for different user settings. It is observed that the cells' average SOC can be charged to close to the desired SOC with the designed optimal charging currents. The effectiveness of the designed optimal charging current scheduling strategy on cell equalization is also demonstrated.

High C-rate current charging: Since the cells have large internal resistances (shown in Fig. 5(b)) in the simulation, the charging currents are limited to be less than 1 C-rate to prevent the overvoltage phenomenon as illustrated in Fig. 6, although the maximum allowed charging current are set as 3 C-rate. To demonstrate how the designed charging scheme performs under higher C-rate, the internal resistances are set as 10% of the original values in the simulation. The desired SOC and the charging duration are set as $\Gamma_{set} = 100\%$ and $T_{set} = 20$ min, respectively. The cells' SOCs, charging currents, terminal voltages and temperatures are illustrated in Fig. 7. The cells' largest charging currents are as high as 3 C-rate, and the cells' average SOC increases to 94.14% after $T_{set} = 20$ min charging. The cells' maximum temperature is about 38.8°C in the charging process, which satisfies the actual thermal constraints. The results demonstrates that fast charging with high C-rate current can be performed while satisfying all charging constraints with setting a short charging duration in our proposed charging strategy.

Effect of weights: In the multi-objective cost function, the weight coefficients represent the relative importance of each objective. A large $\gamma_1/\gamma_2/\gamma_3$ puts more emphasis on charging task/cell equalization/temperature consideration. In the battery charging process, the charging task to satisfy the user demand is the most important, which indicates that a large γ_1 is needed. To evaluate the effects of weights on the charging performance, different γ_2 and γ_3 are adopted in the simulation. Firstly, $\gamma_1 = 1000$ and $\gamma_3 = 0.01$ are chosen, and γ_2 is selected as 0.05, 0.1, 0.5, 1, 5, 10, 20, and 30, respectively. The simulation results in terms of the cells' average SOCs, SOC differences, and average temperatures are illustrated in Figs.

This article has been accepted for publication in a future issue of this journal, but has not been fully edited. Content may change prior to final publication. Citation information: DOI 10.1109/TII.2018.2825245, IEEE Transactions on Industrial Informatics

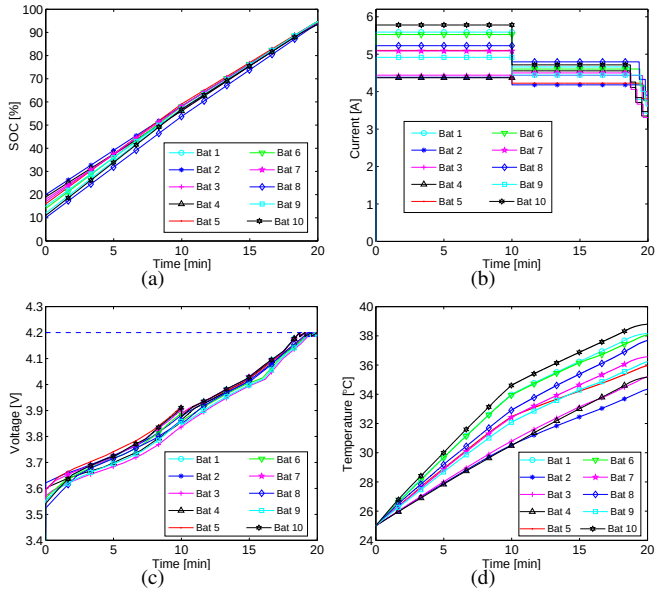

Fig. 7. Simulation results of cells' (a) SOCs with $T_{set} = 20$ min, (b) charging currents with $T_{set} = 20$ min, (c) terminal voltages with $T_{set} = 20$ min, (d) temperatures with $T_{set} = 20$ min.

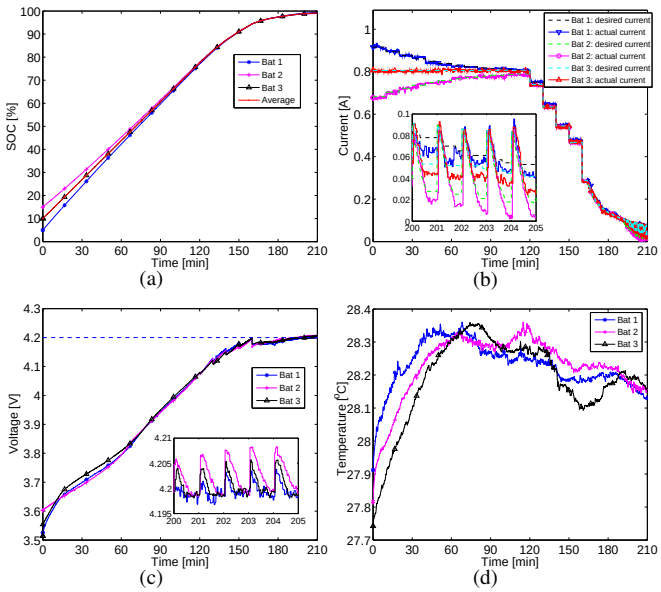

Fig. 9. Experimental results of (a) cells' SOC responses, (b) charging currents, (c) terminal voltages, (d) temperatures.

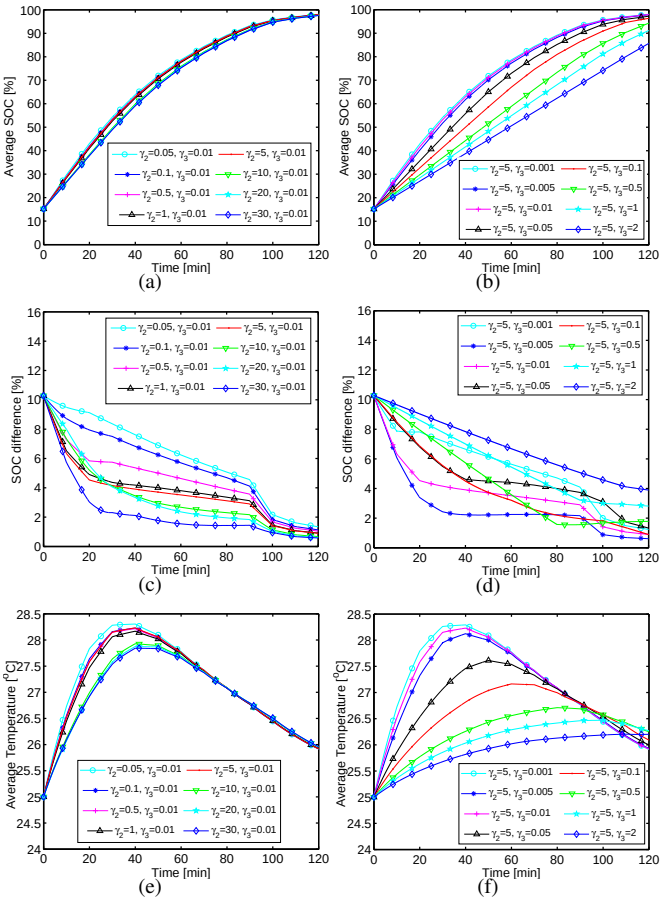

Fig. 8. Simulation results of cells' (a) average SOCs with different γ_2, (b) average SOCs with different γ_3, (c) SOC differences with different γ_2, (d) SOC differences with different γ_3, (e) average temperatures with different γ_2, (f) average temperatures with different γ_3.

8(a), 8(c), and 8(e). It is seen that less SOC difference can be obtained with a large γ_2, which agrees with the above analysis. But excessive γ_2 may reduce the performance of the charging task. Then, $\gamma_1 = 1000$ and $\gamma_2 = 5$ are selected, and a new set of γ_3 is chosen as 0.001, 0.005, 0.05, 0.1, 0.5, 1, and 2, respectively. As shown in Figs. 8(b), 8(d), and 8(f), a large γ_3 can bring less cells' average temperature, but may result in insufficient charging of the battery pack. Overall, the results show a rule that a large γ_2/γ_3 can bring less cells' SOC difference/temperature, but may impact the performance of the charging task to charge the cells' SOCs to their desired value. Users can choose the suitable weights according to this general rule and use the simulation performance as a guide for the weight selection to balance these objectives in practice.

B. Experimental Results

To further validate the effectiveness of the proposed modified isolated buck converter based multi-module battery charger and the hierarchical control based optimal multi-objective charging strategy, several experiments are conducted on the aforementioned three-modular battery pack. The initial SOCs of the battery cells are randomly set as $[5\%, 15\%, 10\%]$, which is obtained by discharging them from the fully-charged states. The cells' maximum allowed charging current is chosen as 0.5 C-rate, which is recommended by the manufacturer. The desired SOC of the battery pack is chosen as $\Gamma_{set} = 100\%$, and the charging duration is set as $T_{set} = 210$ min, respectively. The proposed charging current scheduling algorithm is run using GPIC board, which takes about two seconds.

With a simple internal resistance based battery model utilized in the optimal charging current scheduling algorithm, it may bring bias compared with the cells' actual dynamics. Due to the existence of the model bias, the cells' terminal voltages easily exceed their constraints (16) with the scheduled charging currents when the cells are charged to be near the fully-charged states, as depicted in Figs. 9(a) and 9(c).

However, through reducing the charging currents by a specific rate $\alpha = 5\%$ each time if the cells' measured voltages are larger than the voltage bound, the cells' terminal voltages can be quickly pushed to the value close to 4.2 V, which validates the advantage of the on-line charging current adjusting strategy. The desired charging currents and the actual charging current responses of the multi-module chargers are illustrated in Fig. 9(b). It shows the proposed IDA-PBC can be well used to regulate the actual charging currents via the charger to track their desired values. The cells' SOC responses are illustrated in Fig. 9(a), with the average SOC of 99.16% at the end of the charging process ($SOC_1 = 99.45\%, SOC_2 = 98.94\%, SOC_3 = 99.09\%$), which is close to the desired value. The cells' SOC difference decreases from 7.07% to 0.37%. It demonstrates that the designed hierarchical control based optimal multi-objective charging strategy can satisfy the charging objectives of the user demand and the cell equalization. In traditional charging strategies without cell equalization, all cells are provided with the same charging current in the battery pack. If adopted for this pack, they would force the charging process to be terminated when the second cell is fully charged ($SOC_2 = 100\%$) to avoid overcharge while the first and third cells' SOCs are only $SOC_1 = 91.67\%$ and $SOC_3 = 95.29\%$ (average SOC is 95.65% and SOC difference is 5.91%). It shows the advantage of our designed charging strategy with cell equalization compared with these traditional strategies, which can enhance the effective capacity of the battery pack. The cells' temperatures are measured by the OMEGA temperature sensors, which are maintained in a suitable range of $[27.7^{\circ}\mathrm{C}, 28.4^{\circ}\mathrm{C}]$ in the charging process as illustrated in Fig. 9(d).

V. CONCLUSION

Charging control is critical for the performance and safety of batteries and has received much attention in recent years. This work performs a systematic study of optimal charging control. It begins with the design of a modified isolated buck converter based multi-module charger, which allows each cell of a serially connected battery pack to be individually controlled for charging. A hierarchical charging control approach is developed for the proposed charger. It features a two-layer structure. At the top layer, a multi-objective optimization problem is formulated to schedule the optimal charging current profile concurrently accounting for user demand, cell equalization and temperature effects. Then, control design is accomplished at the bottom layer for the multi-module charger such that it can track the scheduled charging current profile. The proposed charger and multi-objective control approach are thoroughly evaluated through extensive simulation and experiments. Our future work will focus on extending the proposed strategy to more sophisticated battery models to further improve the charging performance.

REFERENCES

[1] O. Kraa, M. Becherif, M. Ayad, R. Saadi, M. Bahri, A. Aboubou, and I. Tegani, "A novel adaptive operation mode based on fuzzy logic control of electrical vehicle," *Energy Procedia*, vol. 50, pp. 194–201, 2014.

[2] S. Mukhopadhyay and F. Zhang, "A high-gain adaptive observer for detecting Li-ion battery terminal voltage collapse," *Automatica*, vol. 50, no. 3, pp. 896–902, 2014.

[3] H. Kim and K. G. Shin, "DESA: Dependable, efficient, scalable architecture for management of large-scale batteries," *IEEE Trans. on Ind. Inform.*, vol. 8, no. 2, pp. 406–417, May 2012.

[4] X. Hu, C. Zou, C. Zhang, and Y. Li, "Technological developments in batteries: a survey of principal roles, types, and management needs," *IEEE Power Energy M.*, vol. 15, no. 5, pp. 20–31, Sept 2017.

[5] Y. Wang, H. Fang, L. Zhou, and T. Wada, "Revisiting the state-of-charge estimation for Lithium-ion batteries: A methodical investigation of the extended Kalman filter approach," *IEEE Control Syst.*, vol. 37, no. 4, pp. 73–96, Aug 2017.

[6] S. Muhammad, M. U. Rafique, S. Li, Z. Shao, Q. Wang, and N. Guan, "A robust algorithm for state-of-charge estimation with gain optimization," *IEEE Trans. on Ind. Inform., in press, doi: 10.1109/TII.2017.2699219*, 2017.

[7] J. Chen, Q. Ouyang, C. Xu, and H. Su, "Neural network-based state of charge observer design for Lithium-ion batteries," *IEEE Trans. Control Syst. Technol.*, vol. 26, no. 1, pp. 313–320, 2018.

[8] H. T. Lin, T. J. Liang, and S. M. Chen, "Estimation of battery state of health using probabilistic neural network," *IEEE Trans. on Ind. Inform.*, vol. 9, no. 2, pp. 679–685, May 2013.

[9] F. Baronti, G. Fantechi, R. Roncella, and R. Saletti, "High-efficiency digitally controlled charge equalizer for series-connected cells based on switching converter and super-capacitor," *IEEE Trans. on Ind. Inform.*, vol. 9, no. 2, pp. 1139–1147, May 2013.

[10] Q. Ouyang, J. Chen, J. Zheng, and Y. Hong, "SOC estimation-based quasi-sliding mode control for cell balancing in Lithium-ion battery packs," *IEEE Trans. Ind. Electron.*, vol. 65, no. 4, pp. 3427–3436, 2017.

[11] Y. Ren, Z. Yu, and G. Song, "Thermal management of a Li-ion battery pack employing water evaporation," *J. Power Sour.*, vol. 360, pp. 166–171, 2017.

[12] A. A.-H. Hussein and I. Batarseh, "A review of charging algorithms for nickel and Lithium battery chargers," *IEEE Trans. Veh. Technol.*, vol. 60, no. 3, pp. 830–838, March 2011.

[13] S. Zhang, K. Xu, and T. Jow, "Study of the charging process of a LiCoO2-based Li-ion battery," *J. Power Sour.*, vol. 160, no. 2, pp. 1349–1354, 2006.

[14] A. Abdollahi, X. Han, G. Avvari, N. Raghunathan, B. Balasingam, K. Pattipati, and Y. Bar-Shalom, "Optimal battery charging, part I: Minimizing time-to-charge, energy loss, and temperature rise for OCV-resistance battery model," *J. Power Sour.*, vol. 303, pp. 388–398, 2016.

[15] K. Liu, K. Li, Z. Yang, C. Zhang, and J. Deng, "An advanced lithium-ion battery optimal charging strategy based on a coupled thermoelectric model," *Electrochim. Acta*, vol. 225, pp. 330–344, 2017.

[16] S. S. Zhang, "The effect of the charging protocol on the cycle life of a Li-ion battery," *J. Power Sour.*, vol. 161, no. 2, pp. 1385–1391, 2006.

[17] Y. H. Liu, C. H. Hsieh, and Y. F. Luo, "Search for an optimal five-step charging pattern for Li-ion batteries using consecutive orthogonal arrays," *IEEE Trans. Energy Convers.*, vol. 26, no. 2, pp. 654–661, 2011.

[18] X. L. D. G. Y. Y. T. Z. H. Min, W. Sun and Z. Zhao, "Research on the optimal charging strategy for li-ion batteries based on multi-objective optimization," *Energies*, vol. 10, no. 5, pp. 1–15, 2017.

[19] R. A. Aliev, R. R. Aliev, B. Guirimov, and K. Uyar, "Dynamic data mining technique for rules extraction in a process of battery charging," *Appl. Soft Comput.*, vol. 8, no. 3, pp. 1252–1258, 2008.

[20] J. Yan, G. Xu, H. Qian, Y. Xu, and Z. Song, "Model predictive control-based fast charging for vehicular batteries," *Energies*, vol. 4, no. 8, pp. 1178–1196, 2011.

[21] X. Hu, S. Li, H. Peng, and F. Sun, "Charging time and loss optimization for LiNMC and LiFePO4 batteries based on equivalent circuit models," *J. Power Sour.*, vol. 239, pp. 449–457, 2013.

[22] Z. Guo, B. Y. Liaw, X. Qiu, L. Gao, and C. Zhang, "Optimal charging method for Lithium ion batteries using a universal voltage protocol accommodating aging," *J. Power Sour.*, vol. 274, pp. 957–964, 2015.

[23] C. Zou, X. Hu, Z. Wei, and X. Tang, "Electrothermal dynamics-conscious Lithium-ion battery cell-level charging management via state-monitored predictive control," *Energy*, vol. 141, pp. 250–259, 2017.

[24] C. Zhang, J. Jiang, Y. Gao, W. Zhang, Q. Liu, and X. Hu, "Charging optimization in Lithium-ion batteries based on temperature rise and charge time," *Appl. Energ.*, vol. 194, pp. 569–577, 2017.

[25] K. Liu, K. Li, and C. Zhang, "Constrained generalized predictive control of battery charging process based on a coupled thermoelectric model," *J. Power Sour.*, vol. 347, pp. 145–158, 2017.

[26] C. Zou, X. Hu, Z. Wei, T. Wik, and B. Egardt, "Electrochemical estimation and control for lithium-ion battery health-aware fast charging," *IEEE Trans. Ind. Electron., in press, doi: 10.1109/TIE.2017.2772154*, 2017.
[27] H. M. J. Z. K. Liu, K. Li and Q. Peng, "Multi-objective optimization of charging patterns for lithium-ion battery management," *Energ. Convers. Manage.*, vol. 159, pp. 151–162, 2018.
[28] A. Fotouhi, D. J. Auger, K. Propp, S. Longo, and M. Wild, "A review on electric vehicle battery modelling: From Lithium-ion toward Lithium-sulphur," *Renew. Sust. Energ. Rev.*, vol. 56, pp. 1008–1021, 2016.
[29] X. Lin, A. G. Stefanopoulou, Y. Li, and R. D. Anderson, "State of charge imbalance estimation for battery strings under reduced voltage sensing," *IEEE Trans. Control Syst. Technol.*, vol. 23, no. 3, pp. 1052–1062, 2015.
[30] J. Zeng, Z. Zhang, and W. Qiao, "An interconnection and damping assignment passivity-based controller for a DC-DC boost converter with a constant power load," *IEEE Trans. Ind. Appl.*, vol. 50, no. 4, pp. 2314–2322, July 2014.
[31] H. Fang, Y. Wang, and J. Chen, "Health-aware and user-involved battery charging management for electric vehicles: Linear quadratic strategies," *IEEE Trans. Control Syst. Technol.*, vol. 25, no. 3, pp. 911–923, 2017.
[32] S. Boyd and L. Vandenberghe, *Convex optimization*. New York, NY, USA: Cambridge university press, 2004.
[33] H. K. Khalil, *Nonlinear Systems*, 3rd ed. Englewood Cliffs, NJ, USA: Prentice Hall, 2002.

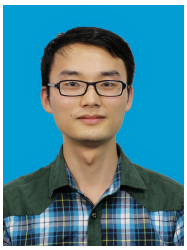

Quan Ouyang Quan Ouyang was born in 1991 in Hubei Province, China. He received the B. S. degree from Huazhong University of Science and Technology in 2013. He is currently a doctoral student in the State Key Laboratory of Industrial Control Technology, College of Control Science and Engineering, Zhejiang University. His research interests include battery management, modeling and control of Fuel Cell system, optimal control, and nonlinear control.

Jian Chen Jian Chen (M'06-SM'10) received the B.E. and M.E. degrees from Zhejiang University, Hangzhou, China, in 1998 and 2001, respectively, and the Ph.D. degree in electrical engineering from Clemson University, Clemson, SC, USA, in 2005. He was a Research Fellow with the University of Michigan, Ann Arbor, MI, USA, from 2006 to 2008, where he was involved in fuel cell modeling and control. He joined IdaTech LLC, Bend, OR, USA, in 2008, where he was involved in fuel cell back power systems, and Proterra Inc., Greenville, SC, USA, in 2012, where he was involved in the National Fuel Cell Bus Program. In 2013, he joined the Department of Control Science and Engineering, Zhejiang University, where he is currently a Professor with the College of Control Science and Engineering. His research interests include modeling and control of fuel cell vehicles, battery management, visual servo techniques, and nonlinear control.

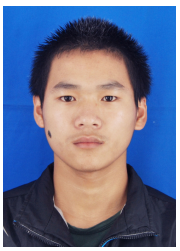

Jian Zheng Jian Zheng was born in 1995 in Jiangxi Province, China. He received the bachelors degree in automation from Huazhong University of Science and Technology, Wuhan, China in 2016. He is currently pursuing the M.E. degree in the State Key Laboratory of Industrial Control Technology, College of Control Science and Engineering, Zhejiang University. His current research interests include battery management and nonlinear control.

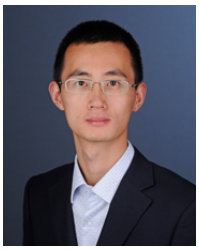

Huazhen Fang Huazhen Fang (M'14) is an Assistant Professor of Mechanical Engineering at the University of Kansas. He received his Ph.D. degree in Mechanical Engineering from the Department of Mechanical & Aerospace Engineering at the University of California, San Diego (2014). Prior to that, he received M.Sc. in Mechanical Engineering from the University of Saskatchewan, Canada (2009), and B.Eng. in Computer Science & Technology from Northwestern Polytechnic University, China (2006). He worked as a Research Intern at Mitsubishi Electric Research Laboratories and NEC Laboratories America, respectively, in 2012 and 2013. His research interests lie in control and estimation theory with application to energy management, environmental observation, system prognostics and mechatronics. He has served as Associate Editor, Program Committee Member and Session Organizer for a few international conferences, including American Control Conference, ASME Dynamic Systems and Control Conference, IEEE Conference on Control Technology & Applications, IEEE International Conference on Industrial Informatics, IEEE Conference on Control & Automation, etc. He co-guest edited for the Focused Section on Advanced Control and Navigation for Marine Mechatronic Systems, IEEE/ASME Transactions on Mechatronics. He was a recipient of the Outstanding Reviewer Award of IEEE Transactions on Cybernetics in 2016.